

Probing Light-stimulated Activities in the Retina via Transparent Graphene Electrodes

Xiaosi Zhang¹, Hannah Lee², Yuchen Zhang¹, Thayer S. Walmsley³, Deyu Li^{4,}, Edward
Levine^{2,5,*}, Ya-Qiong Xu^{1,3}*

¹Department of Electrical and Computer Engineering, Vanderbilt University, Nashville,
TN 37235, USA

²Department of Ophthalmology and Visual Sciences, Vanderbilt Eye Institute, Vanderbilt
University Medical Center, Nashville, TN 37235, USA

³Department of Physics and Astronomy, Vanderbilt University, Nashville, TN 37235, USA

⁴Department of Mechanical Engineering, Vanderbilt University, Nashville, TN 37235,
USA

⁵Department of Cell and Developmental Biology, Vanderbilt University, Nashville, TN
37235, USA

*E-mail: deyu.li@vanderbilt.edu

*E-mail: ed. ed.levine@vumc.org

Abstract

Graphene has triggered tremendous research due to its superior properties. In particular, the intrinsic high light transmission illustrates the unique advantage in neural biosensing. Here, we combine perforated flexible graphene electrodes with microfluidic platforms to explore real-time extracellular electrical activities of retinal ganglion cells (RGCs). Under light stimulation, the transparent graphene electrodes have demonstrated the capability of recording the electrical activities of stimulated RGCs in direct contact. Different types of RGCs have shown three distinct light induced patterns: ON, OFF, and ON-OFF, which are primarily operated by cone photoreceptors. Moreover, the observed spiking waveforms can be divided into two groups: the biphasic waveform usually occurs at contacts with soma, while the triphasic waveform is likely related to the axon. Under high K^+ stimulation, the graphene electrodes exhibit higher electrical sensitivity than gold counterparts with an average 2.5-fold enhancement in spiking amplitude. Furthermore, a strong response has been observed with the firing rate first increasing and then ceasing, which could be due to the potassium-induced neural depolarization. These results show that graphene electrodes can be a promising candidate in the electrophysiology studies of retina and offer a route to engineering future two-dimensional materials-based biosensors.

Keywords: Graphene, retina, electrical activities, light stimulation, spiking waveform sorting, K^+ stimulation

Introduction

The retina, like many other parts of the central nervous systems, contains massive neurons of various types. These neurons with extended dendrites and axons, form parallel yet interactive neural building blocks, detect and deliver the output information to the brain, making it an ideal candidate in electrophysiology studies.¹⁻⁴ Several layers of neurons are connected by synapses in the retina; and the primary light-sensing layer including cones and rods responds to light stimulation. The retinal ganglion cells (RGCs) extend to form an optic nerve that convey visual information as an electrical signal processed by the retinal circuits. Such a unique neural connection, cell morphologies, and information processing mechanisms make the exploration of their electrical activities imperative to understand how these units achieve higher functions such as sight and cognition.

Various techniques have been developed to study the electrical activities in the retina. The patch-clamp technique has been widely used to record intracellular action potentials and their associated response to extracellular stimulations of the retinal neurons, which offers sub-millisecond temporal resolution but is limited in spatial resolution because of the sizable probes and bulky manipulator.⁵⁻⁶ It has also been demonstrated that fluorescent calcium indicators can be utilized to optically record electrical activities in retinal cells with a high spatial resolution at the micrometer range.⁷⁻⁸ However, the electrical sensitivities are significantly lower than the patch-clamp method. Microelectrode arrays (MEA), which integrate high-density probing electrodes in one device, can simultaneously record spiking activity of RGCs from multiple channels.⁹ More importantly, it provides a platform to realize real-time electrophysiological measurements. Recently, two-dimensional (2D) materials (e.g. graphene) have been shown to exhibit great

potential in electrophysiology and neuroimaging.¹⁰ Adopting transparent graphene electrodes in MEA could offer several advantages, especially for retinal neuron recording. The flexibility of graphene enables easy integration with flexible substrates while maintaining high performance. Its biocompatibility allows for direct contact with biological fluids and tissues, which can be employed in both *in vivo* and *ex vivo* conditions.¹¹⁻¹³ In addition, the 2D nature of graphene with the whole volume exposed to the environment makes it extremely sensitive to surface charge changes.¹⁴⁻¹⁵ Last but not least, the transparent nature of flexible graphene electrodes facilitates direct light modulation to targeted RGCs in comparison with traditional opaque electrodes.¹⁶⁻¹⁷ The novel mechanical, electrical, and optical properties as well as the applications in electronics and optoelectronics offered by graphene, are well suited to create a revolutionary platform for retinal neurological research.

In this paper, we integrate transparent graphene probes with a microfluidic platform to record the extracellular electrical activities of RGCs in explanted whole retina. Two stimulation methods have been utilized in our experiments. Under photopic light illumination, the spiking activities of RGCs as a result of cone response have shown three different patterns: ON, OFF, and ON-OFF. Furthermore, various waveforms have been detected, in which biphasic spiking waveforms may result from direct contact with somas while triphasic spiking waveforms are likely attributed to isolated axons. Under high K^+ stimulation, the spiking activities detected by graphene electrodes illustrate an average 2.5 times higher amplitude than gold electrodes. And an obvious increase in the action potential firing rate has been observed, which is likely due to the potassium-induced depolarization. Our experimental

results shed light on understanding the functions of RGCs and open up new avenues for probing the retina through highly sensitive, flexible, and transparent 2D materials-based devices.

Methods

Graphene growth and characterization. Graphene layers were grown using a standard chemical vapor deposition (CVD) method.¹⁸ We loaded the copper foil on a quartz boat into a furnace system after the copper film was rinsed with nitric acid for 10 minutes. The copper foil was annealed at 1000°C with 100 sccm hydrogen for 1 h after the system was pumped down to 10 mTorr. Then graphene was grown on the copper foil at 1000°C in the presence of 20 sccm of methane and 80 sccm of hydrogen for 30 minutes. The intensity and layer information for the graphene was characterized by Raman with a 532 nm laser source.

Transparent graphene electrode fabrication and microfluidic platform configuration. Four-inch silicon wafers were used as support substrates to build transparent graphene electrodes. First, we spin coated 10 μm -thick polyimide (PI-2611, HD Microsystems) on the wafers and cured it under nitrogen atmosphere at 250°C to prevent fracturing of the film. Polyimide was chosen as the substrate material due to its stable thermal properties, adequate mechanical property, and good biocompatibility. Next, patterned metal electrodes (Ti/Au, 10 nm/100 nm) was deposited by e-beam evaporation followed by a lift-off process. Then, the polyimide substrate and holes were structured simultaneously through a dry etching process by Trion Phantom II with the thick SPR220-7.0 photoresist as an etching mask so that the flexible probes can be mechanically peeled off from the silicon substrate. Subsequently, we transferred the as-grown monolayer graphene onto the target area by using the bubbling transfer method.¹⁹ The graphene pattern

was defined by the standard photolithography and etching with O₂ plasma. Finally, SU-8 (SU-8 2002 MicroChem), a permanent epoxy-based negative photoresist, was used to passivate the metal area with the open graphene window defined.

The microfluidic probing platform consisted of two glass slides, parafilm, plastic tubing, graphene sensor film, and glass ring. First, two glass slides and a patterned parafilm were used to form a sandwich structure with a fluid chamber and channel in between. Two holes were drilled on the top glass slide and the graphene sensor film was glued on the center area of one hole while a plastic tubing was attached to the other hole. Withdrawing fluid from the tube helps create a negative pressure in the fluid channel to allow for retina to be gently attached to the graphene sensor film. Finally, a glass ring was glued on the top glass slide to form a reservoir.

***Ex vivo* recordings, data analysis and retina preparation.** The graphene electrode film was clamped to a zero-insertion-force connector which was a lab-made printed circuit board. A flat flexible cable with a desired shape was used as a substrate to support and align I/O pad arrays. Electrical recordings were obtained through a commercially available voltage recording setup, a 16-channel amplifier (RHD2132, Intan Technologies). Recordings were acquired at a 20 kHz sampling rate. The sorting procedures used in this work were conducted in the Plexon Offline V4 sorter.

Animals. The welfare of the mice and the procedures used for this study are in accordance with the Association for Research in Vision and Ophthalmology (ARVO) guidelines and the American Association for Accreditation of Laboratory Animal Care (AAALAC). All procedures were approved by the Vanderbilt University IACUC under the protocol M1600235. Mice were maintained on a 12-hour light cycle and were euthanized

approximately 4.5 hours following light onset (9:30 AM). Euthanasia was performed by carbon dioxide inhalation until respiration ceased and immediately followed by cervical dislocation.

Retina preparation. The eyes were excised immediately following cervical dislocation and quickly submerged into gassed (95% O₂ and 5% CO₂) Ames medium. Retinas were isolated and dissected under dim red illumination to minimize photopigment bleaching. The retina was then incubated in Ames medium containing collagenase (241 u/mL, Sigma-Aldrich Corporation) and hyaluronidase (1,370 u/mL, Worthington Biochemical Corporation) for 10 minutes at room temperature. Next, the digested retina was washed with Ames media, mounted photoreceptor side down on Whatman 3MM Chr cellulose paper (Fisher Scientific) and transferred to the MEA device such that the RGC layer was in direct contact with the graphene electrodes.

Results and Discussion

Fabrication and characterization of graphene electrodes. Graphene microelectrodes were fabricated on a 10 μm-thick flexible polyimide substrate. Figure 1a shows the optical image of typical transparent graphene probes and gold counterparts of the same size. Evenly distributed holes are patterned in the sensing region of the polyimide substrate. A perforated polyimide film allows for better physical contact than non-perforated MEAs, enables nutrients to easily reach the bottom RGC layer, and fixates the tissue during the experiment. The almost symmetric perforations ensure uniform detection results to facilitate comparison between the graphene and gold electrodes. Additionally, the film has a hole to surface area ratio of ~23%, which has been shown to provide optimal

contact.²⁰ As-grown graphene membranes were transferred to desired areas. The graphene was patterned by O₂ plasma, followed by coating of a SU8 passivation layer to define an activate area of either 80×80 μm² or 20×20 μm² for each electrode to detect the local electrochemical environments. Raman spectroscopy measurements revealed the quality and thickness of graphene with a 532 nm laser. The 2D-to-G intensity ratio is about 2, indicating the monolayer structure of the as-grown graphene (Figure 1b).²¹⁻²³ We note that while monolayer graphene was used in this work, few layer graphene electrodes may also be suitable as long as high optical transparency is maintained. One major advantage of graphene electrodes is their high optical transparency (>90%) as compared to other electrodes like ITO (80%) and ultra-thin metals (60%),²⁴ which allows for recording the electrical signals while conducting direct light stimulation and real-time imaging.

***Ex vivo* retina recordings with transparent graphene electrodes.** To explore the extracellular electrical activity of the RGC layer, we performed *ex vivo* whole retina recordings with transparent graphene electrodes. As shown in Figure 1c, the transparent graphene electrodes were placed into a microfluidic platform and connected with a zero-insertion force connector to interface with recording electronics (see details in Methods). The microfluidic chamber and channel underneath the graphene electrodes is connected to a media withdraw cannula (the blue tube in Figure 1c), which creates a negative pressure in the fluidic chamber. On top of the graphene electrodes, one perfusion cannula providing media (red tubing in Figure 1c) is inserted into the retina well and a suction cannula is placed near the top of the retina well to prevent overflow (green tubing in Figure 1c). To start the experiment, the whole system was perfused with carbogen-bubbled Ames media with a peristaltic pump controlling the flow rate and a heated cannula controlling the

temperature to be around 36°C. The retina tissue was then transferred into the well with RGCs atop electrodes, after which we engaged a pump to draw media through the blue tube connected to the fluidic channel to create a negative pressure underneath the retina. This negative pressure induces media perfusion through the perforated polyimide substrate, which allows for the retina tissue to be gently pulled towards the graphene electrodes. This procedure can enhance the physical contact between the retina tissue and the electrodes. Additionally, the fresh solution can reach the bottom cell layers to provide sufficient oxygenation and nutrient. Neural data were collected at a 20 kHz sampling rate from 16 channels via an Intan Recording System. Figure 1d shows typical spontaneous spiking activities recorded from one channel of transparent graphene probes. The zoom-in view of a single spike indicates that it is likely the extracellular action potential of a RGC body (Figure 1e).

Light induced stimulation to retina. Light stimulation was applied to the retina to investigate the associated electrical response by using transparent graphene electrodes. Photoreceptors such as rods and cones inside the retina layers can detect the light and trigger electrical signals propagating through the retinal circuits.²¹ RGCs have large receptive fields, receiving input from multiple photoreceptors via a diverse collection of interneurons. Processing of the visual signal is also mediated through different circuit configurations, neurotransmitter profiles, and neuromodulation, all of which ultimately influence the nature of the RGC response. Light incident on the retina is primarily absorbed by photosensitive chemicals in the rods and cones, which trigger neurotransmitter release through the horizontal, bipolar, and amacrine cell levels, to the RGCs. In the simplest iteration, RGCs respond to light in one of three ways, by firing action potentials in response

to light, the on-response, by firing action potentials when illumination is stopped, the off-response, and by firing action potentials in response to the onset and termination of illumination, the on-off response.²⁵

Owing to the high light transmissivity of graphene, we are able to employ light from the bottom through the graphene electrodes, which allows for direct detection of the related response of RGCs. This light stimulation can be reflected by the electrical spiking changes measured by the graphene electrodes. As shown in Figure 2, we were able to observe three distinct patterns of firing rate distributions under 1 s white light stimulation, showcasing all three types of RGC responses (ON, OFF, ON-OFF). Figure 2 also displays the corresponding raster plots of RGC firing and the time interval between each light stimulation cycle is 60 s. Distinctions also exist among the ON and OFF patterns. The transient type can generate or vanish a burst of spikes, while the sustained firing type could persist more than the light stimulus period. For ON-OFF RGCs, it fires both when light is turned on and off (Figure 2e).²⁶ Figure 2f is the frequency distribution of the RGC types recorded in the experiment. Approximately half of RGCs exhibit ON response under 1 s full-field stimulation, in agreement with the previous retina study.²⁷ The light intensity applied to the retina was $3.5 \log \text{ cd/m}^2$, which was photopic illumination.²⁸ Therefore, the visual response of the retina is primarily from cone photoreceptors.²⁹ In general, the ON and OFF RGCs driven by the changes in excitatory and inhibitory inputs are related to different pathways in the retinal circuitry.³⁰⁻³¹

In addition, different electrical spiking waveforms were recorded by transparent graphene electrodes (Figure 3), which was likely related to various cell morphologies, synaptic connectivity, and relative position to the electrode. According to the shape and

frequency, recorded spiking waveforms can be divided into two groups: biphasic and triphasic waveforms. The biphasic waveforms are commonly classified into either regular-spiking (RS) or fast-spiking (FS) patterns, in which RS tends to have a wider waveform (Figure 3a) compared to FS (Figure 3b). Triphasic-spiking (TS) and compound-spiking (CS) exhibit triphasic characteristics with a large positive-first phase (Figure 3d and 3e).³² TS and CS has two positive spikes with a significant negative trough. The second positive peak of the CS is slightly wider than TS.³³ According to the extracellular action potential model based on the volume conductor theory, a biphasic waveform is likely associated with the cell body (soma), while a triphasic waveform tends to be detected from an isolated axon.³⁴⁻³⁵ The local point where the action potential flows into acts as a sink, while the point where the action potential flows away provides a current source. When a spike is initiated at the soma, a negative voltage is measured when the soma first acts as a sink during the depolarization process. After the action potential travels away from the soma down to the axon, the cell body serves as the source, leading to a positive voltage (Figure 3c). For the axon, the membrane under the electrode is a source for the nearby depolarized signal, thus producing a positive voltage. When the action potential reaches the electrode, a negative voltage is detected. Then, the contact area becomes an ion source again after the potential action moves away (Figure 3f).³⁶⁻³⁷

Extracellular high K⁺ concentration stimulation. After the characterization of the light-induced electrical activities, extracellular potassium was applied to investigate the related response of the retina. The 22 mM K⁺ media was introduced from the perfusion loops by using a peristaltic pump to control the flow rate. The potassium stimulant lasted for 150 s before switching the loop back to the baseline Ames medium. A strong response

was observed with potassium exposure followed by a depletion period before the spontaneous activity returned. Figure 4a and 4b illustrate the median biphasic waveform and the firing spike rate of the action potential with a timestamp, respectively. To further analyze the response frequencies, a box-and-whisker plot is used to quantitatively compare the firing rate between the spontaneous and K^+ stimulated spiking (Figure 4c). A similar trend of potassium-stimulated response was observed when the recording activities demonstrated a triphasic behavior (Figure 4d, e, f). Both types of spiking waveforms show a significant increase in firing rates during potassium stimulation due to enhanced neuronal depolarization. The neuronal membrane voltage is mainly regulated by the concentration of potassium and sodium ions inside and outside the cell membrane. At rest, an intracellular membrane voltage was negative, and the potassium ion was present in much higher concentrations inside the cell while the sodium ion concentrations were oppositely distributed. The movement of the ions across the membrane is naturally controlled by voltage-gated potassium and sodium channels.³⁸ However, exposing the neuron to high levels of extracellular potassium reverse the chemical gradient, causing the positive K^+ to move inside the cell, and the voltage inside the cell begins to increase, which is called potassium-induced depolarization.³⁹ This depolarization process made the voltage inside the cells relatively easy to reach the threshold, causing a significant increase in action potential firing rates.⁴⁰ However, the sustained depolarization eventually caused inactivation of voltage-gated channels and prevented the action potential from firing.⁴¹ Following removal of the high potassium media, the RGCs returned to spontaneous spiking after approximately 130 seconds. Moreover, Figure 4g, h shows spiking activities of RGCs recorded from a graphene and a gold electrode under high K^+ stimulation, respectively.

The spiking amplitude detected by the graphene electrode is about 2.5-fold compared to the one with a gold electrode of the same size, demonstrating higher electrical sensitivity in this retina experiment.

Conclusion

In this work, we use a perforated transparent graphene probe to perform electrophysiology measurements on mouse retinal tissues. Distinct ON, OFF, and ON-OFF responses from RGCs have been observed under light stimulation, which can be attributed to different optical pathways primarily mediated by cones. Various spiking waveforms with biphasic and triphasic characteristics are recorded, which are likely associated with different regions of neurons, such as soma and axon. We also demonstrate that the action potential spiking firing rate for the retina greatly increases under the high K^+ stimulation, which is induced by neural depolarization. Our experimental results suggest that transparent graphene probes exhibit higher electrical sensitivity. Together with previously demonstrated flexibility and biocompatibility,^{15, 42} we believe that graphene electrodes are promising for the detection of the electrical activities of the retina and offer an opportunity to investigate electrical behaviors of other neural networks.

AUTHOR INFORMATION

Corresponding Authors

E-mail: deyu.li@vanderbilt.edu

E-mail: ed.levine@vumc.org

ORCID

Deyu Li: 0000-0001-8364-0924

Notes

The authors declare no competing financial interest.

Y.X. is deceased

Acknowledgements

This paper is dedicated to Dr. Y.-Q. Xu who passed away during the manuscript review process.

We would like to thank Dr. Sharon M Weiss and Dr. Michael Risner for helpful discussions. This work was supported by the National Institutes of Health (1R01EY027729) and the National Science Foundation (ECCS-1810088). Device fabrication was partially conducted at the Center for Nanophase Materials Sciences, which is a DOE Office of Science User Facility.

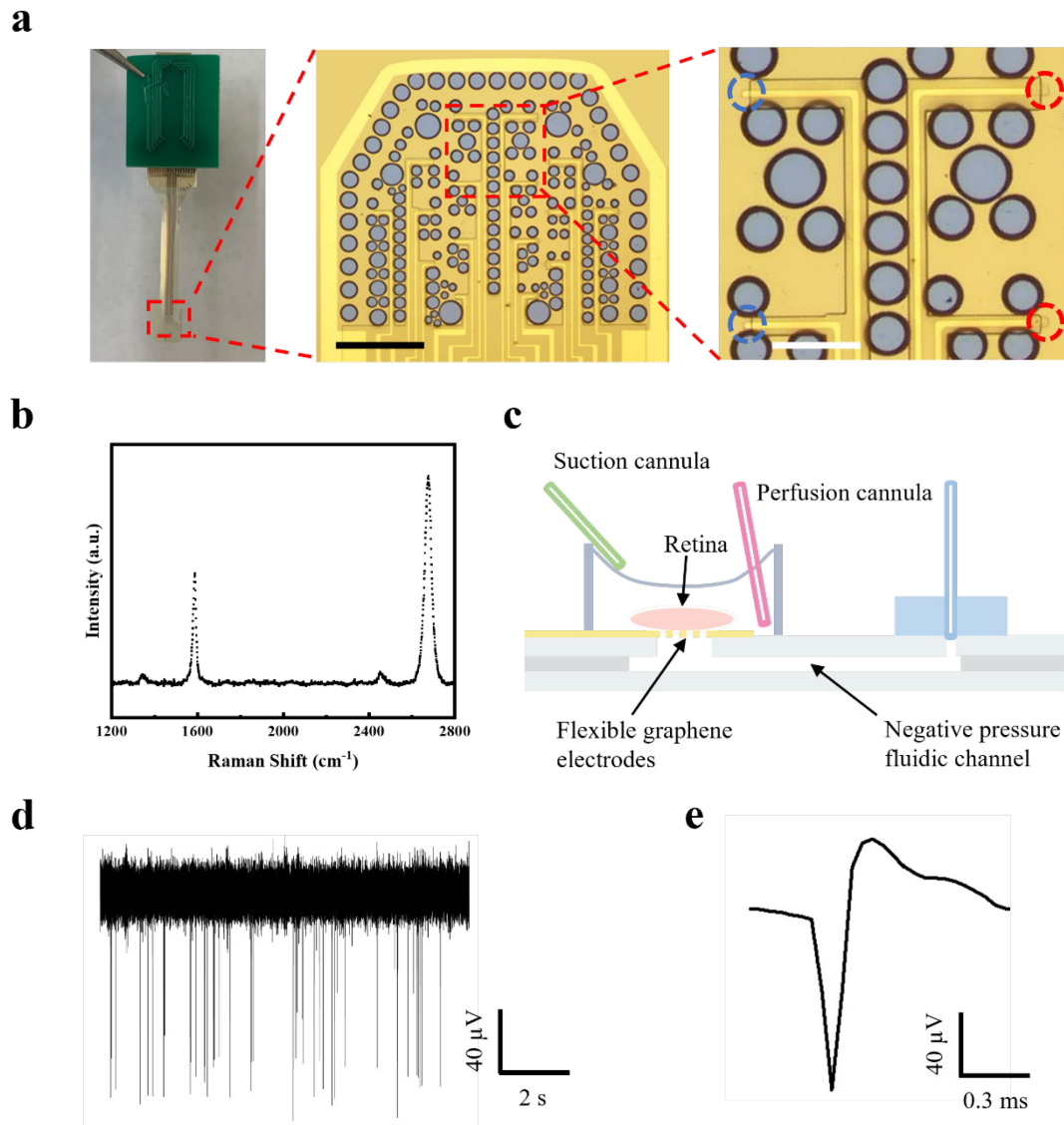


Figure 1. (a) Optical image of flexible probes with graphene electrodes and gold electrodes, which are marked by red and blue circles, respectively. The electrode size is $20 \times 20 \mu\text{m}^2$. Scale bar is $500 \mu\text{m}$ and $200 \mu\text{m}$, respectively. (b) Raman spectrum of as-grown graphene under 532 nm illumination. (c) Schematic diagram of a graphene-based microfluidic platform. The light grey plates represent glass slides while the darker grey plate indicates the patterned parafilm. The red and green tubing represents perfusion and suction cannula, respectively. The blue structure illustrates the tubing connected to a media withdraw pump.

(d) Typical spontaneous spiking activities of RGCs recorded by transparent graphene probes. (e) A representative zoom-in view of a single spiking waveform from RGCs.

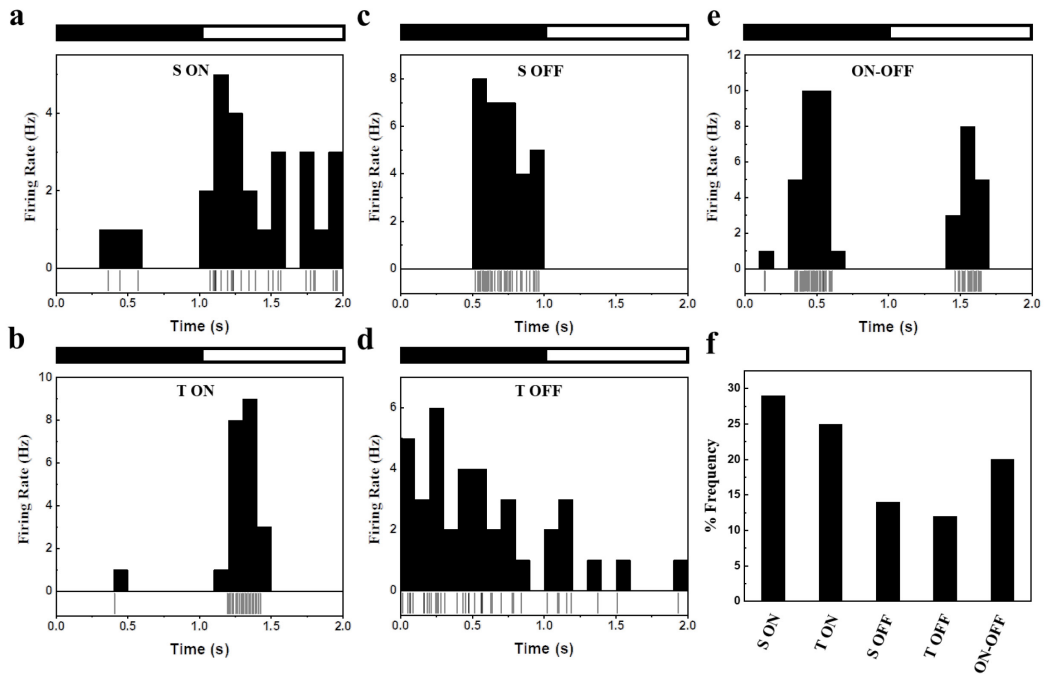


Figure 2. Response types of RGCs to light stimulation: (a) sustained ON, (b) transient ON, (c) sustained OFF, (d) transient OFF, and (e) ON-OFF. Each diagram shows a representative histogram and raster plot of the firing rate distributions under 1 s full-field illumination. Bars above the plots show the light OFF (black bar) or ON (white bar). (f) Frequency distribution of the RGC types.

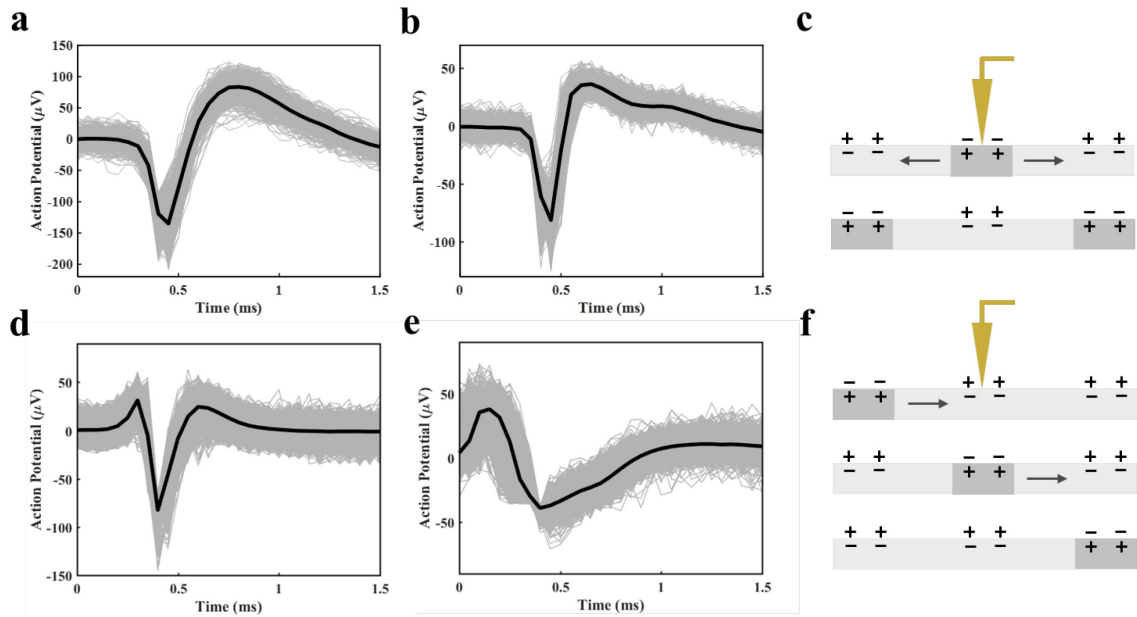


Figure 3. Typical biphasic spiking waveforms: (a) regular-spiking and (b) fast-spiking. Typical triphasic spiking waveforms: (d) triphasic-spiking and (e) compound-spiking. Lighter lines indicate all spikes recorded from one experiment cycle while black lines are the extracted median waveform. Extracellular action potential models for (c) biphasic and (f) triphasic waveform spikes, respectively. The light gray boxes represent RGCs with the charge distributed inside and outside the cell membrane, while the dark box highlights the position that the action potential is located. The orange indicator illustrates an external recording electrode while the black arrow shows the propagation direction of the action potential on the soma and axon. The illustrations in each panel are in a temporal order.

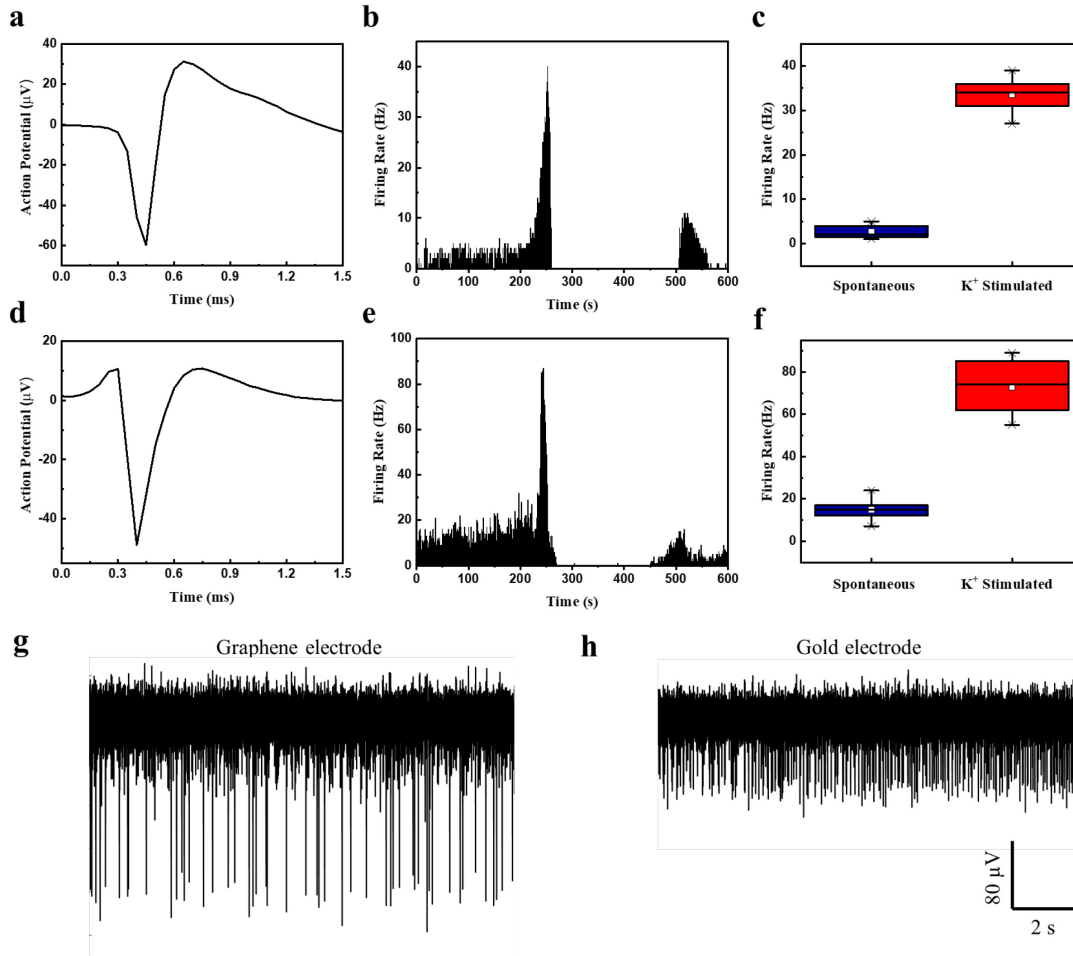
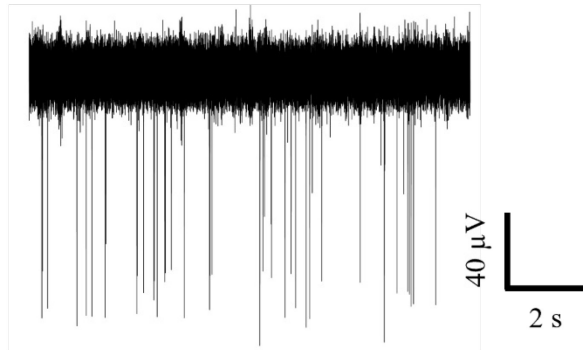
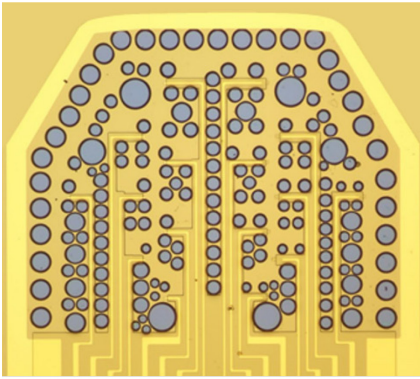


Figure 4. Representative median spikes: (a) biphasic and (d) triphasic waveforms of RGCs under high K^+ stimulation. (b) and (e) are corresponding histograms of action potential firing rates as a function of time under high K^+ stimulation. (c) and (f) are related box-and-whisker plots of firing rate distributions of spontaneous activity and under high K^+ stimulation, respectively. In the charts, the box ends indicate the first and third quartiles while whiskers mark the 5% and 95% margins. The middle line and the small square in the box represent the median and mean values, respectively. In addition, crosses depict the minimum and maximum values. Spiking activities of RGCs detected from (g) a graphene and (h) a gold electrode under K^+ stimulation. The figures shown here are representative data from three independent experiments.

TOC graphic



References

- (1) Schwartz, E. A.; Tachibana, M. Electrophysiology of glutamate and sodium co-transport in a glial cell of the salamander retina. *J. Physiol.* **1990**, *426* (1), 43-80.
- (2) Fujiwara, T.; Imamura, Y.; Margolis, R.; Slakter, J. S.; Spaide, R. F. Enhanced Depth Imaging Optical Coherence Tomography of the Choroid in Highly Myopic Eyes. *Am. J. Ophthalmol* **2009**, *148* (3), 445-450.
- (3) Iseri, P. K.; Altinas, Ö.; Tokay, T.; Yüksel, N. Relationship between Cognitive Impairment and Retinal Morphological and Visual Functional Abnormalities in Alzheimer Disease. *J. neuro-ophthalmology* **2006**, *26* (1), 18-24.
- (4) Timmers, A. M.; Zhang, H.; Squitieri, A.; Gonzalez-Pola, C. Subretinal injections in rodent eyes: effects on electrophysiology and histology of rat retina. *Mol. Vis.* **2001**, *7*, 131-7.
- (5) Ohkuma, M.; Kawai, F.; Horiguchi, M.; Miyachi, E. Patch-clamp recording of human retinal photoreceptors and bipolar cells. *Photochem. Photobiol.* **2007**, *83* (2), 317-22.
- (6) Bodoia, R. D.; Detwiler, P. B. Patch-clamp recordings of the light-sensitive dark noise in retinal rods from the lizard and frog. *J. Physiol.* **1985**, *367* (1), 183-216.
- (7) Denk, W.; Detwiler, P. B. Optical recording of light-evoked calcium signals in the functionally intact retina. *Proc. Natl. Acad. Sci.* **1999**, *96* (12), 7035-7040.
- (8) Behrend, M. R.; Ahuja, A. K.; Humayun, M. S.; Weiland, J. D.; Chow, R. H. Selective labeling of retinal ganglion cells with calcium indicators by retrograde loading in vitro. *J. Neurosci. Methods.* **2009**, *179* (2), 166-172.
- (9) Tsai, D.; Sawyer, D.; Bradd, A.; Yuste, R.; Shepard, K. L. A very large-scale microelectrode array for cellular-resolution electrophysiology. *Nat. Commun.* **2017**, *8* (1), 1802.
- (10) Kuzum, D.; Takano, H.; Shim, E.; Reed, J. C.; Juul, H.; Richardson, A. G.; de Vries, J.; Bink, H.; Dichter, M. A.; Lucas, T. H.; Coulter, D. A.; Cubukcu, E.; Litt, B. Transparent and flexible low noise graphene electrodes for simultaneous electrophysiology and neuroimaging. *Nat. Commun.* **2014**, *5* (1), 5259.
- (11) Hossain, R. F.; Deaguero, I. G.; Boland, T.; Kaul, A. B. Biocompatible, large-format, inkjet printed heterostructure MoS₂-graphene photodetectors on conformable substrates. *npj 2D Mater. Appl.* **2017**, *1* (1), 28.
- (12) Zhang, Y.; Dodson, K. H.; Fischer, R.; Wang, R.; Li, D.; Sappington, R. M.; Xu, Y.-Q. Probing electrical signals in the retina via graphene-integrated microfluidic platforms. *Nanoscale* **2016**, *8* (45), 19043-19049.
- (13) Cheng, Z.; Li, Q.; Li, Z.; Zhou, Q.; Fang, Y. Suspended Graphene Sensors with Improved Signal and Reduced Noise. *Nano Lett.* **2010**, *10* (5), 1864-1868.
- (14) Schedin, F.; Geim, A. K.; Morozov, S. V.; Hill, E. W.; Blake, P.; Katsnelson, M. I.; Novoselov, K. S. Detection of individual gas molecules adsorbed on graphene. *Nat. Mater.* **2007**, *6* (9), 652-655.
- (15) Masvidal-Codina, E.; Illa, X.; Dasilva, M.; Calia, A. B.; Dragojević, T.; Vidal-Rosas, E. E.; Prats-Alfonso, E.; Martínez-Aguilar, J.; De la Cruz, J. M.; Garcia-Cortadella, R.; Godignon, P.; Rius, G.; Camassa, A.; Del Corro, E.; Bousquet, J.; Hébert, C.; Durduran, T.; Villa, R.; Sanchez-Vives, M. V.; Garrido, J. A.; Guimerà-Brunet, A. High-resolution mapping of infraslow cortical brain activity enabled by graphene microtransistors. *Nat. Mater.* **2019**, *18* (3), 280-288.

- (16) Park, D.-W.; Brodnick, S. K.; Ness, J. P.; Atry, F.; Krugner-Higby, L.; Sandberg, A.; Mikael, S.; Richner, T. J.; Novello, J.; Kim, H.; Baek, D.-H.; Bong, J.; Frye, S. T.; Thongpang, S.; Swanson, K. I.; Lake, W.; Pashaie, R.; Williams, J. C.; Ma, Z. Fabrication and utility of a transparent graphene neural electrode array for electrophysiology, in vivo imaging, and optogenetics. *Nat. Protoc.* **2016**, *11* (11), 2201-2222.
- (17) Nair, R. R.; Blake, P.; Grigorenko, A. N.; Novoselov, K. S.; Booth, T. J.; Stauber, T.; Peres, N. M. R.; Geim, A. K. Fine Structure Constant Defines Visual Transparency of Graphene. *Science (New York, N.Y.)* **2008**, *320* (5881), 1308-1308.
- (18) Wang, R.; Shi, M.; Brewer, B.; Yang, L.; Zhang, Y.; Webb, D. J.; Li, D.; Xu, Y.-Q. Ultrasensitive Graphene Optoelectronic Probes for Recording Electrical Activities of Individual Synapses. *Nano Lett.* **2018**, *18* (9), 5702-5708.
- (19) Rosa, C. J. L. d. I.; Sun, J.; Lindvall, N.; Cole, M. T.; Nam, Y.; Löffler, M.; Olsson, E.; Teo, K. B. K.; Yurgens, A. Frame assisted H₂O electrolysis induced H₂ bubbling transfer of large area graphene grown by chemical vapor deposition on Cu. *Appl. Phys. Lett.* **2013**, *102* (2), 022101.
- (20) Reinhard, K.; Tikidji-Hamburyan, A.; Seitter, H.; Idrees, S.; Mutter, M.; Benkner, B.; Münch, T. A. Step-by-step instructions for retina recordings with perforated multi electrode arrays. *PloS one* **2014**, *9* (8), e106148-e106148.
- (21) Calizo, I.; Bejenari, I.; Rahman, M.; Liu, G.; Balandin, A. A. Ultraviolet Raman microscopy of single and multilayer graphene. *J. Appl. Phys.* **2009**, *106* (4), 043509.
- (22) Berciaud, S.; Ryu, S.; Brus, L. E.; Heinz, T. F. Probing the Intrinsic Properties of Exfoliated Graphene: Raman Spectroscopy of Free-Standing Monolayers. *Nano Lett.* **2009**, *9* (1), 346-352.
- (23) Chen, S.; Moore, A. L.; Cai, W.; Suk, J. W.; An, J.; Mishra, C.; Amos, C.; Magnuson, C. W.; Kang, J.; Shi, L.; Ruoff, R. S. Raman Measurements of Thermal Transport in Suspended Monolayer Graphene of Variable Sizes in Vacuum and Gaseous Environments. *ACS Nano* **2011**, *5* (1), 321-328.
- (24) Park, D.-W.; Schendel, A. A.; Mikael, S.; Brodnick, S. K.; Richner, T. J.; Ness, J. P.; Hayat, M. R.; Atry, F.; Frye, S. T.; Pashaie, R.; Thongpang, S.; Ma, Z.; Williams, J. C. Graphene-based carbon-layered electrode array technology for neural imaging and optogenetic applications. *Nat. Commun.* **2014**, *5* (1), 5258.
- (25) Dowling, J. E. *The retina: an approachable part of the brain*, Harvard University Press: 1987.
- (26) Vaney, D. I.; Sivyer, B.; Taylor, W. R. Direction selectivity in the retina: symmetry and asymmetry in structure and function. *Nat. Rev. Neurosci.* **2012**, *13* (3), 194-208.
- (27) Nirenberg, S.; Meister, M. The light response of retinal ganglion cells is truncated by a displaced amacrine circuit. *Neuron* **1997**, *18* (4), 637-50.
- (28) Zele, A. J.; Cao, D. Vision under mesopic and scotopic illumination. *Front. Psychol.* **2014**, *5*, 1594.
- (29) Umino, Y.; Solessio, E.; Barlow, R. B. Speed, spatial, and temporal tuning of rod and cone vision in mouse. *J. Neurosci.* **2008**, *28* (1), 189-98.
- (30) Chalupa, L. M.; Günhan, E. Development of On and Off retinal pathways and retinogeniculate projections. *Prog. Retin. Eye Res.* **2004**, *23* (1), 31-51.
- (31) van Wyk, M.; Wässle, H.; Taylor, W. R. Receptive field properties of ON- and OFF-ganglion cells in the mouse retina. *Vis. Neurosci.* **2009**, *26* (3), 297-308.

- (32) Fogli Iseppe, A.; Ogata, G.; Johnson, J. S.; Partida, G. J.; Johnson, N.; Passaglia, C. L.; Ishida, A. T. Extraretinal Spike Normalization in Retinal Ganglion Cell Axons. *eneuro* **2020**, *7* (2), ENEURO.0504-19.2020.
- (33) Sun, S. H.; Almasi, A.; Yunzab, M.; Zehra, S.; Hicks, D. G.; Kameneva, T.; Ibbotson, M. R.; Meffin, H. Analysis of extracellular spike waveforms and associated receptive fields of neurons in cat primary visual cortex. *J. Physiol.* **2021**, *599* (8), 2211-2238.
- (34) Rutkove, S. B. Introduction to Volume Conduction. In *The Clinical Neurophysiology Primer*; Blum, A. S.; Rutkove, S. B., Eds.; Humana Press: Totowa, NJ, 2007; pp 43-53.
- (35) Bakkum, D. J.; Frey, U.; Radivojevic, M.; Russell, T. L.; Müller, J.; Fiscella, M.; Takahashi, H.; Hierlemann, A. Tracking axonal action potential propagation on a high-density microelectrode array across hundreds of sites. *Nat. Commun.* **2013**, *4* (1), 2181.
- (36) Barry, J. M. Axonal activity in vivo: technical considerations and implications for the exploration of neural circuits in freely moving animals. *Front. Neurosci.* **2015**, *9* (153).
- (37) Nam, Y.; Wheeler, B. C. In vitro microelectrode array technology and neural recordings. *Crit. Rev. Biomed. Eng.* **2011**, *39* (1), 45-61.
- (38) Rienecker, K. D. A.; Poston, R. G.; Saha, R. N. Merits and Limitations of Studying Neuronal Depolarization-Dependent Processes Using Elevated External Potassium. *ASN neuro* **2020**, *12*, 1759091420974807.
- (39) Tolón, R. M.; Sánchez Franco, F.; de los Frailes, M. T.; Lorenzo, M. J.; Cacicedo, L. Effect of potassium-induced depolarization on somatostatin gene expression in cultured fetal rat cerebrocortical cells. *J. Neurosci.* **1994**, *14* (3 Pt 1), 1053-9.
- (40) Golbs, A.; Nimmervoll, B.; Sun, J. J.; Sava, I. E.; Luhmann, H. J. Control of programmed cell death by distinct electrical activity patterns. *Cereb. Cortex.* **2011**, *21* (5), 1192-202.
- (41) Cannon, S. C.; H. Brown, R.; Corey, D. P. A sodium channel defect in hyperkalemic periodic paralysis: Potassium-induced failure of inactivation. *Neuron* **1991**, *6* (4), 619-626.
- (42) Fischer, R. A.; Zhang, Y.; Risner, M. L.; Li, D.; Xu, Y.; Sappington, R. M. Impact of Graphene on the Efficacy of Neuron Culture Substrates. *Adv. Healthc. Mater.* **2018**, *7* (14), e1701290.